Journal of Materials Chemistry C

Accepted Manuscript

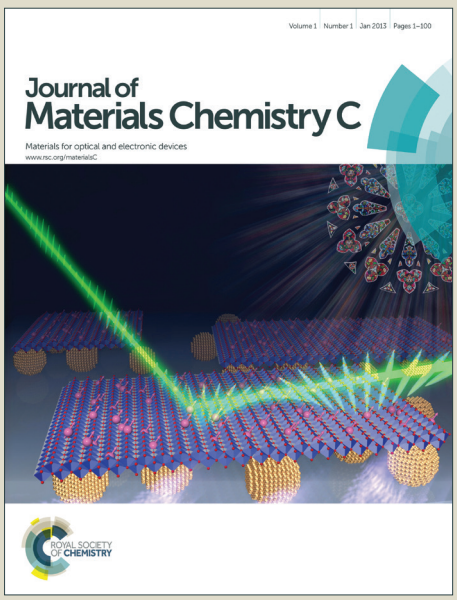

ROYAL SOCIETY OF CHEMISTRY

www.rsc.org/materialsC

Photovoltaic Performance Enhancement of P3HT/PCBM Solar Cells Driven by Incorporation of Conjugated Liquid Crystalline Rod-coil Block Copolymers

Kai Yuan[1], Lie Chen[1], Yiwang Chen*[1,2]

[1]Institute of Polymers/Department of Chemistry, Nanchang University, 999 Xuefu Avenue, Nanchang 330031, China; [2]Jiangxi Provincial Key Laboratory of New Energy Chemistry, Nanchang University, 999 Xuefu Avenue, Nanchang 330031, China

ABSTRACT

The potential application of poly-3-hexylthiophene (P3HT) based liquid crystalline rod-coil block copolymers in polymer solar cells has been investigated. The two liquid crystalline copolymers bearing a rodlike liquid crystal block poly-(4-(dodecyloxy)-4''-(oct-7-en-1-yloxy)-1,1':4',1''-terphenyl), **(P3HT-*b*-Pterph)**, and a discotic liquid crystal block poly-(2,3,6,7,10-pentakis(hexyloxy)-11-(oct-7-en-1-yloxy)triphenylene), **(P3HT-*b*-PTP)**, respectively. The solar cells based on the two self-assemble liquid crystalline block copolymers blend with [6,6]-phenyl-C_{61}-butyric acid methyl ester (PCBM) show poor photovoltaic performance due to the introduction of the low conductive non-conjugated liquid crystalline block. The devices performance was improved after thermal treatment at liquid crystalline temperature originating from the self-orientation of the liquid crystalline block copolymers and the formation of well-organized domains in the blend. However, utilization of the liquid crystalline block copolymers as compatibilizers in P3HT:PCBM blends, the morphology combined with the photovoltaic performance of P3HT:PCBM solar cells can be significantly improved after annealing from the liquid crystalline states. It is demonstrated that the self-assembly of liquid crystalline block located the donor and acceptor interface can enhance crystallization and ordering of P3HT chains and guarantee the formation of interpenetrating networks, subsequently resulting in the improvement of efficient exciton separation of the active layer. The copolymer with

* Corresponding author. Tel.: +86 791 83969562; fax: +86 791 83969561. *E-mail address*: ywchen@ncu.edu.cn (Y. Chen).

the discotic liquid crystal block is more favorable than the one with rodlike liquid crystal block, due to the more compatible with the fullerene acceptors and the more efficient charge transport caused by self-assembled columnar phase from the discotic liquid crystals. Therefore, the optimized morphology and promoted charge mobility improved the short-circuit current density and fill factor to give the power conversion efficiency up to 4.03%.

Keywords: Liquid crystals; block copolymers; self-assemble; compatibilizers; crystallization

1. Introduction

Organic photovoltaic (OPV) solar cells composed of the conjugated polymer donor and fullerene derivative acceptor have spurred worldwide attention in the past two decades, because of their potential for low-cost renewable energy source, flexible and facility large scale manufacturing by printing.[1-4] The power conversion efficiency (PCE) has been significantly improved over 9% for single cells and 10% for multi-junction cells.[5-7] Despite continuous improvement in PCE, the overall performance of conjugated polymer donor and fullerene derivatives based solar cells is still limited by many drawbacks, such as the difficulty in developing the desired nanomorphology of active layer for efficient charge separation and transportation, and the thermal instability on morphology during long term annealing.[8-10] Further advancement on performance and the stability of device is thus required to satisfy commercialization.[11,12]

In bulk heterojunction (BHJ) solar cells, the local conjugated polymer ordering, fullerene derivatives agglomeration and the phase separation between the donor and acceptor are directly correlated to the performance of devices.[8,13] Thereby, a continuous nanoscale interpenetrating network structure of active layer is crucial for high performance BHJ solar cells with promoted stability. The nature of conjugated block copolymers molecular architecture comprising a rod-like conjugated block and a coil-like block with additional functionalities enable themselves self-assemble into a various of highly organized and thermodynamically stable morphologies,[14-16] which is regarded as an effective strategy for controlling such microphase separation morphology of the active layers.[14,16,17] Utilization of the block copolymers in BHJ solar cells to manage the micromorphology is primarily through three approaches. Firstly, the self-assembled block copolymers based on donor and acceptor building blocks were used as active layer alone.[18] Secondly, block copolymer donors were blended with fullerene derivatives acceptor to form BHJ active layer.[19,20] However, the PCE of the devices based on both mentioned methods is very low ascribed to the too high fraction of insulating moiety introduced into the block copolymers chain. Incorporation of block copolymers as compatibilizers in conjugated polymer/fullerene

derivatives blends is found to be the most prospective approach for obtaining the desired active layer morphology. [9,13,21-23]

Liquid crystalline materials have been studied extensively due to their unique electronic and optoelectronic properties.[24-27] It has been reported that introduction of liquid crystalline block into block copolymers could arrange the copolymers with a well-organized nanostructures owing to the nature of mesoscopic ordering.[25,26] The degree of molecular orientation of the liquid crystalline conjugated block copolymer can be further enhanced by an external perturbation such as shear stress, electric or magnetic field.[26] Therefore, liquid crystalline materials have drawn extensive attention in the field of OPV,[27-29] including some work in our groups.[30-36] High performance of solar cells was achieved through the intermolecular and mesoscopic ordering of liquid crystalline materials, especially annealed at the liquid crystalline state.[33,35]

Herein, we extend our previous works and report on two poly-3-hexylthiophene (P3HT) based liquid crystalline rod-coil block copolymers bearing a poly-(4-(dodecyloxy)-4''-(oct-7-en-1-yloxy)-1,1':4',1''-terphenyl) block **(P3HT-*b*-Pterph)** and a poly-(2,3,6,7,10-pentakis(hexyloxy)-11-(oct-7-en-1-yloxy)triphenylene) block **(P3HT-*b*-PTP)**, respectively, and their application in polymer solar cells. The solar cells based on the two self-assemble liquid crystalline block copolymers blended with PCBM show poor photovoltaic performance, even after thermal treatment at liquid crystalline temperature, due to the low conductivity of the non-conjugated liquid crystalline block. However, when utilize the liquid crystalline block copolymers as compatibilizers in P3HT:PCBM blends, the photovoltaic performance of P3HT:PCBM solar cells can be significantly improved after liquid crystalline state annealing. The self-assemble liquid crystalline block copolymers can induce the crystallinity of P3HT, and cocrystallize with P3HT chains, resulting in a long range crystallinity of P3HT domain. On the other hand, the liquid crystalline block located at the interface of the P3HT and PCBM domains can promote the formation of the favorable interpenetrating networks. The modified crystallization and ordering of

P3HT chains thus guarantee the efficient charge mobility of the active layer. The optimized morphology and enhanced hole-, electron- mobility consequently led to the improved PCE up to 4.03%.

2. Experimental section

P3HT-*b*-Pterph and **P3HT-*b*-PTP** were synthesized through atom-transfer radical polymerization (ATRP) using bromoester terminated P3HT macroinitiator (**P3HT-Br**) as initiator (**Scheme 1**), CuBr and 1,1,4,7,10,10-hexamethyl triethylene tetramine (HMTETA) as catalyst and ligand, respectively. **P3HT-Br** was fabricated according to a procedure of previous literature.[37] The polymerization was performed at the molar ratio of [monomer **A** or **B**] : [CuBr] : [P3HT-Br] : [HMTETA] = 100 : 1 : 1 : 2. **P3HT-Br** (0.11 g, 0.01 mmol) and monomer **A** or **B** (10 mmol) were dissolved in toluene in a dry flask filled with nitrogen. After the mixture was stirred for 30 min, the flask was immersed into a preheated oil bath at 90 ^{o}C. Then, HMTETA (5 μL, 0.02 mmol) and CuBr (1.46mg, 0.01 mmol) were added to the reaction mixture to react overnight. Then, the reaction mixture was cooled down and precipitated by pouring into methanol. The liquid crystalline block copolymers were collected by filtrating under reduced pressure. The polymers were purified by Al_2O_3 column and sequential Soxhlet extractions with methanol, hexane, and chloroform. The polymers were isolated via precipitated in methanol. The liquid crystalline block copolymers were characterized by ^{1}H NMR. **P3HT-*b*-Pterph**, ^{1}H NMR (600 MHz, $CDCl_3$) δ (ppm): 7.60-7.55 (m, 8H), 6.98 (m, 5H), 4.00 (t, 4H), 2.90 (m, 2H), 1.8-1.68 (m, 9H), 1.56-1.27 (m, 34H), , 0.92 (t, 6H). **P3HT-*b*-PTP**, ^{1}H NMR (600 MHz, $CDCl_3$) δ (ppm): 7.84 (s, 6H), 6.98 (s, 1H), 4.23 (t, 12H), 2.68 (d, 2H), 1.87-1.58 (m, 17H), 1.50-1.25 (m, 42H), 0.92 (t, 18H). (The detailed experimental procedures and characterization of the monomers and polymers are given in the Supporting Information.)

The solar cell device was fabricated as the following steps. Indium tin oxide (ITO) coated glass (15 Ω/square) substrates were firstly patterned (15 mm×15 mm) and etched. Then, the ITO substrates were cleaned by ultrasonic in deionized water,

acetone and isopropyl alcohol sequentially each for 20 min. The cleaned ITO substrates were treated with plasma for 10 minutes. The solutions of liquid crystalline block copolymers and PCBM were prepared by dissolving **P3HT-*b*-Pterph** or **P3HT-*b*-PTP** and PCBM (1:1 w/w) in 1,2-dichlorobenzene (DCB) at a concentration of **P3HT-*b*-Pterph** or **P3HT-*b*-PTP** being 10 mg/mL, then the solutions were stirred at 50 ^{o}C in glove box overnight. The P3HT/**P3HT-*b*-Pterph** or **P3HT-*b*-PTP**/PCBM ternary solutions were prepared by introducing **P3HT-*b*-Pterph** or **P3HT-*b*-PTP** into P3HT/PCBM (1:1 w/w) DCB solution with the **P3HT-*b*-Pterph** or **P3HT-*b*-PTP** concentrations varying from 0 to 10 wt % with respect to the amount of P3HT:PCBM, where the concentration of P3HT is 10 mg/mL. In order to promote complete dissolution, the solutions were stirred at 50 ^{o}C in glove box overnight. The conventional architectures of devices were glass/ITO/PEDOT:PSS/active layer/LiF/Al. A 30 nm poly(ethylenedioxythiophene) : polystyrene sulphonate (PEDOT:PSS, Baytron P VP A1 4083) was spin-coated on ITO glass at 4000 rpm for 60 s. The PEDOT:PSS coated substrates were heated at 140 ^{o}C for 10 minutes in air to dry. The mixed **P3HT-*b*-Pterph** or **P3HT-*b*-PTP**/PCBM solution or P3HT/**P3HT-*b*-Pterph** or **P3HT-*b*-PTP**/PCBM solution was spin-coated on the top of PEDOT:PSS layer at a spin rate of 800 rpm for 60 s. After the films dried, a top metal cathode (1 nm LiF and 100 nm Al) was thermal evaporated by a shadow mask to complete the device fabrication.

Structural analysis of the monomers and polymers were performed by using ^{1}HNMR spectroscopy (600 MHz Varian spectrometer), using deuterated chloroform ($CDCl_3$) as a solvent, tetramethylsilane (TMS) as internal standard. The UV-vis-NIR spectroscopy (performed by Perkin-Elmer Lambda 750 with integrating sphere) and photoluminescence spectrometer (Hitachi F-7000) were employed to shed light on the photophysics and electronic properties of **P3HT-*b*-Pterph**, **P3HT-*b*-PTP** and all the active layers. The time-resolved photoluminescence (TRPL, Edinburgh Instrument FLS920) was employed to determine the photoluminescence decay with a H_2 gas lamp as the light source. The nanostructures of the active layers and **P3HT-*b*-Pterph**, **P3HT-*b*-PTP** were confirmed by atomic force microscope (AFM, Digital

Instrumental Nanoscope 31) and transmission electron microscopy (TEM; JEOL, JEM-2100F, field emission transmission electron microscope). The peak currents were measured by conductive atomic force microscopy (CAFM) using peak force tapping tunneling AFM (Bruker, MultiMode 8, PeakForce TUNA). The thermostability of the liquid crystalline block copolymers were studied by thermogravimetric analysis (TGA) performed under N_2 with a TA instrument SDT-Q600 thermogravimetric analyzer. Differential scanning calorimetry (DSC, Perkin-Elmer DSC 7 differential scanning calorimeter) was employed to investigate the phase-transition temperatures of the liquid crystalline block copolymers with a constant heating/cooling rate of 5 ^{o}C/min. The texture of the liquid crystalline monomers and block copolymers were observed by polarizing optical microscopy (POM, Nikon E600POL polarizing optical microscope) equipped with an Instec HS 400 heating and cooling stage. The out-of-plane grazing incidence X-ray diffraction (GIXD) profiles were carried out by using a Bruker D8 Discover reflector with an X-ray generation power of 40 kV tube voltage and 40 mA tube current. In order to increase the effective X-ray penetrating depth and minimize the background from the substrate scattering, the angle between the incident beam and the film surface was fixed at 0.2°. The testing of current-voltage (*J-V*) characteristics of the devices under illumination and in dark were done by Keithley 2400 Source Meter. The light intensity of the simulated AM 1.5 G illumination (Abet Solar Simulator Sun2000) was 100 mW·cm^{-2}.

3. Results and Discussion

The liquid crystalline rod-coil block copolymers **P3HT-*b*-Pterph** with rodlike terphenyl mesogen and **P3HT-*b*-PTP** with disc triphenylene mesogen were synthesized through "grafting-from" method using a P3HT macroinitiator (**P3HT-Br**). The bromoester terminated P3HT macroinitiator **P3HT-Br** was prepared according to previously reported procedure.[37,38] The liquid crystalline block was grown by atom-transfer radical polymerization (ATRP) of monomer A or B with mesogens,[25,34,39,40] as depicted in **Scheme 1**. The chemical structure and the molar

ratio of the liquid crystalline block copolymers were confirmed by ^{1}H NMR spectroscopy (**Figure S1**), and the molar ratio of P3HT block to liquid crystalline block are 9:1 and 10:1 for **P3HT-*b*-Pterph** and **P3HT-*b*-PTP**, respectively. The molecular weight for **P3HT-*b*-Pterph** and **P3HT-*b*-PTP** are Mw = 14900 and Mw = 16500, respectively. The detailed experimental procedures and structural characterization were provided in the Supporting Information (**Scheme S1, Figure S2, S3**).

The thermal and phase behaviors of the liquid crystalline rod-coil block copolymers **P3HT-*b*-Pterph** and **P3HT-*b*-PTP** were investigated by thermogravimetric analysis (TGA), differential scanning calorimetry (DSC) and polarized optical microscopy (POM), as summarized in **Table 1**. From the TGA (**Figure S4**) we can infer that the **P3HT-*b*-Pterph** and **P3HT-*b*-PTP** began to decompose at about 416 and 403 °C, respectively, and lost most of the weight at about 500 °C, suggesting the good thermal stability. In the DSC measurements (**Figure S5**), both liquid crystalline block copolymers display good reproducible thermograms. The second heating curves of **P3HT-*b*-Pterph** and **P3HT-*b*-PTP** exhibit endothermal peaks at 174.8 and 150.3 °C, associated to their liquid crystalline phase transitions. The nature of the liquid crystallinity can also been verified by the POM microphotographs (**Figure 1**). The monomer A shows a smectic phase while the monomer B possesses a typical texture of columnar phase from heating-cooling cycles. During heating, the two liquid crystalline block copolymers present a birefringent and homogeneous textures during the liquid crystalline states, nevertheless, the mesophase could not be distinguished clearly.[41]

The photoluminescence (PL) and absorption data of the liquid crystalline rod-coil block copolymers were also listed in **Table 1**. **Figure S6** presents the UV-vis absorption spectra of **P3HT-*b*-Pterph** and **P3HT-*b*-PTP** films. The absorption spectra of **P3HT-*b*-Pterph** and **P3HT-*b*-PTP** are basically the same. The two characteristic absorption bands in the absorption spectra correspond to the polythiophene block in the visible light region (~560 nm) and the π-π* transition of the liquid crystalline block in the ultraviolet region around 270 nm. The two liquid crystalline block

copolymers display a sharp shoulder at about 605 nm, indicating that the polythiophene backbones in the block copolymers could self-assemble to the orderly molecular arrangement.[42,43] The self-assemble property of the liquid crystalline rod-coil block copolymers was further supported by transmission electron microscopy (TEM), as shown in **Figure 1**. The **P3HT-*b*-Pterph** and **P3HT-*b*-PTP** thin films show long-range arrangement of highly interconnected fibrillar objects, which is the well-known self-assemble morphological signature for most polythiophene based block copolymers.[44,45] The liquid crystalline block copolymer **P3HT-*b*-Pterph** and **P3HT-*b*-PTP** films show a characteristic PL emission peak at 637 and 642 nm, respectively, originating not from the liquid crystalline moiety but from the polythiophene backbones.[46]

The optical bandgaps estimated from UV-vis absorption spectra onset for **P3HT-*b*-Pterph** and **P3HT-*b*-PTP** are 1.88 and 1.90 eV, respectively. The highest occupied molecular orbital (E_{HOMO}) of **P3HT-*b*-Pterph** and **P3HT-*b*-PTP** are determined at 5.35 and 5.30 eV from the onset oxidation potential of the corresponding cyclic voltammograms (**Figure S7**). The lowest unoccupied molecular orbital (E_{LUMO}) of **P3HT-*b*-Pterph** and **P3HT-*b*-PTP** calculated from the values of optical bandgaps and E_{HOMO} are 3.47 and 3.40 eV, respectively. These results indicate that the two liquid crystalline block copolymers possess narrow bandgaps and low ionizations, therefore, the photovoltaic performance based on the liquid crystalline block copolymers could be expected.

The potential application in the solar cells of the liquid crystalline rod-coil block copolymers was explored. Photovoltaic properties of **P3HT-*b*-Pterph** (or **P3HT-*b*-PTP**):PCBM based solar cells were investigated with the device structure of ITO/PEDOT:PSS/**P3HT-*b*-Pterph** (or **P3HT-*b*-PTP)** :PCBM/LiF/Al. The photovoltaic characteristics of the devices at different thermal treatments under AM 1.5G illumination at 100 mW/cm^2 are summarized in **Table 2**, and the representative current density-voltage (*J-V*) curves are depicted in **Figure S8**. Both of **P3HT-*b*-Pterph** and **P3HT-*b*-PTP** based solar cells exhibit poor PCE of 0.34-0.44% and show anomalous S-shape *J-V* curves with the low fill factors (FFs) in the range of

20-25%, and a short-circuit current density (J_{sc}) of 2.83 and 3.62 mA/cm^2, respectively. As it is known to all that interfaces play a critical role in determining electric field distribution, charge extraction and collection.[47] In this case, the poor conductive of the liquid crystalline block in the copolymers would create a interfacial dipoles or/and hole collection barrier near the anode, subsequently leading to S-shape *J-V* curves and loss of FF and/or J_{sc}.[48]

After thermal annealing, especially from the liquid crystalline states, the devices performance is slightly improved to 0.56 % for **P3HT-*b*-Pterph** and 0.63% for **P3HT-*b*-PTP**. While annealing temperature (200 ^{o}C) is beyond the liquid crystalline states, the devices efficiency dramatically decreases. The change in PCE is mainly contributed from the change in J_{sc} after thermal annealing. **Figure S9** presents the normalized UV-vis absorbance spectra of **P3HT-*b*-Pterph**/PCBM and **P3HT-*b*-PTP**/PCBM active layers before and after annealing at different temperatures. It is evidenced that the optical absorption of the liquid crystalline block copolymers based active layers slightly increased after thermal annealing in the range of liquid crystalline state temperatures. This is because liquid crystalline state annealing promotes the orientation of mesogens to induce the polythiophene backbones packing with higher ordering.[42,49] The enhanced ordering of polymer chains is favoring for charge carrier mobility, thus improving the J_{sc}. On the other hand, as given in **Figure S10**, annealing at liquid crystalline state temperatures induces the most quenched PL of the liquid crystalline block copolymers and PCBM blends, therefore, the improved J_{sc} is also partly from the more efficient exciton dissociation[50]. The improved molecular ordering induced by liquid crystalline state annealing can be verified by the increased dichroism (N_F) in the polarized photoluminescence spectra of the active layers which were determined from the ratio of perpendicular polarization ($F_{\perp}$) to parallel polarization ($F_{//}$), as shown in **Figure S11, S12**, and **Table S1.** Furthermore, surface topography images of the active layers annealed at different temperatures are shown in **Figure 2**. The root mean squared (RMS) roughness for the **P3HT-*b*-Pterph** based active layer extracted from the AFM images decreases from 4.6 nm for as cast to 3.1 nm for annealed from liquid

crystalline state, and then increases after further elevating annealing temperature to 200 ^{o}C. The change in RMS for **P3HT-*b*-PTP** based active layer exhibits the similar tendency. These observations are well consistent with the *J-V* curves shown in **Figure S8**.

Since the rod-coil block copolymers can serve as compatibilizers in polymer solar cells to modify the nanostructure of active layers, and to improve device performance,[9,13,21,22] For the liquid crystalline rod-coil block copolymers **P3HT-*b*-Pterph** and **P3HT-*b*-PTP** as nanostructuring compatibilizers in P3HT:PCBM based solar cells, the assembly of liquid crystals and the molecule-block interaction between P3HT block and P3HT are expected to induce a long range crystallinity of P3HT domain. In addition, due to the π-π interaction between the liquid crystalline block and the fullerene acceptor, liquid crystalline block located at the interface of the P3HT and PCBM can improve the interfacial compatibility and guarantee the formation of the favorable interpenetrating networks. The *J-V* curves of the devices based on P3HT:PCBM:**P3HT-*b*-Pterph** and P3HT:PCBM:**P3HT-*b*-PTP** with various amounts of **P3HT-*b*-Pterph** or **P3HT-*b*-PTP** are shown in **Figure 3**, and the device characteristics were summarized in **Table 3**. Due to the liquid crystalline state annealing optimizing the morphology of the active layer, the devices based on P3HT:PCBM:**P3HT-*b*-Pterph** were performed after postannealing at liquid crystalline state temperature 175 ^{o}C, and P3HT:PCBM:**P3HT-*b*-PTP** devices were annealed at 150 ^{o}C. As shown in **Figure 3** and **Table 3**, incorporation of a small amount of the liquid crystalline block copolymers can greatly improve the J_{sc} and FF of these devices. Among the devices based on P3HT:PCBM:**P3HT-*b*-Pterph** and pristine P3HT:PCBM, incorporated 3 wt% **P3HT-*b*-Pterph** into the active layer achieves the best performance of 3.34±0.15%, together with the J_{sc} increasing from 8.97±0.2 mA/cm^2 to 9.58±0.3 mA/cm^2, and the FF increasing from 45.1±1% to 58.1±1%. Moreover, the devices based on P3HT:PCBM:**P3HT-*b*-PTP** shows the overall improved performance than those based on P3HT:PCBM:**P3HT-*b*-Pterph**. The discotic liquid crystal block in **P3HT-*b*-PTP** is more compatible with the fullerene acceptors, which guarantees the more favorable interpenetrating networks.

On the other hand, the self-assembled columnar phase from the discotic liquid crystals favors the more efficient charge transport. The highest PCE of 4.03±0.15% is achieved when the concentration of **P3HT-*b*-PTP** is 5%, with a J_{sc} = 10.36±0.3 mA/cm^2, and a FF=64.9±1%. A higher weight ratio (10%) of **P3HT-*b*-PTP** leads to a reduced PCE, J_{sc} and FF, due to the too much poor conductive non-conjugated liquid crystalline block.[9]

When doping **P3HT-*b*-PTP** into active layers, the improvement of J_{sc} and FF can be explained by dark *J-V* curves of P3HT:PCBM with various weight fraction of **P3HT-*b*-PTP** solar cells after annealed at 150 ^{o}C (**Figure S13**). The reverse saturation current density decreases upon increasing the concentration of **P3HT-*b*-PTP**, and the 5% weight fraction of **P3HT-*b*-PTP** yields the lowest leakage current. A lower leakage current indicates a less charge losses by trapping and recombination, leading to a larger shunt resistance (R_{sh}) and higher FF.[21,51] The R_{sh} increases from 728.5 Ω cm^2 for pristine P3HT:PCBM to 1074.2Ω cm^2 with the addition of 5% **P3HT-*b*-PTP**. The series resistance (R_s) of the pristine P3HT:PCBM device is around 8.3 Ω cm^2, but reduces to 4.8 Ω cm^2 when incorporated 5% **P3HT-*b*-PTP**, as shown in **Table 3**. Therefore, the increased R_{sh}, reduced R_s and leakage currents should be responsible for the improvement of J_{sc} and FF.

It is widely acknowledged that the conformation, degree of order of the polymer chains in the active layer plays a crucial role in charge separation and transport process.[50,52] The self-assemble liquid crystalline block copolymers can induce the crystallinity of P3HT, and cocrystallize with P3HT chains, resulting in a long range crystallinity of P3HT domain and favorable interpenetrating networks. The conformation, level of orientation of the polymer chains can be evaluated from the electronic absorption spectra of the active layers.[53] The correlation between the optical properties (UV-vis absorption) and the **P3HT-*b*-PTP** fractions of the active layers are highlighted in **Figure 4**. The absorption spectra composed of a high energy region and a low energy region, which are corresponding for amorphous and crystalline state P3HT chains, respectively.[42,54] The P3HT chains are isolated in a flexible coil conformation in the amorphous state P3HT, and linearized π-stacked

chains form weakly interacting H-aggregates in the crystalline state P3HT chains.[55] In the normalized (normalized to 0-2 vibronic transition absorption) absorption spectra, there are three vibronic peaks of $A_{0\text{-}2}$, $A_{0\text{-}1}$ and $A_{0\text{-}0}$ (where subscripts denote respective vibrational quanta coupled to electronic transitions) located at 523, 558 and 608 nm, respectively.[43,54] The presence of the vibronic transition peaks and the intensity of the amplitude ratio are associated to the ordering degree of the P3HT chains and the charge carrier mobility.[19,43,56] Previous literatures have been reported that the presence of the peak at 608 nm suggests the strong π-π interaction between P3HT chains and is indicative of a high degree of crystallinity of P3HT.[56,57] When increasing the fraction of **P3HT-*b*-PTP** from 1% to 5%, the vibronic transition peaks at $A_{0\text{-}1}$ and $A_{0\text{-}0}$ become more pronounced in the absorption spectra. The amplitude ratio of $A_{0\text{-}0}/A_{0\text{-}1}$ and $A_{0\text{-}0}/A_{0\text{-}2}$ of the active layers with various weight ratio of **P3HT-*b*-PTP** are listed in **Table 4**. The $A_{0\text{-}0}/A_{0\text{-}1}$ and $A_{0\text{-}0}/A_{0\text{-}2}$ ratios increase with the concentration of **P3HT-*b*-PTP** increasing, both of which reach the climax when 5% of **P3HT-*b*-PTP** is incorporated into the active layer. The increased $A_{0\text{-}0}/A_{0\text{-}1}$ and $A_{0\text{-}0}/A_{0\text{-}2}$ ratio imply that a small amount of **P3HT-*b*-PTP** could enhance crystallization of P3HT chains. The UV-vis absorption spectra of the P3HT:PCBM and P3HT:PCBM: **P3HT-*b*-Pterph** films with various weight ratio of **P3HT-*b*-Pterph** after annealed at 175 ^{o}C show the similar tendency as presented in **Figure S14.**

To gain deeper insight into the degree of crystalline and local intrachain ordering with the fraction ratio of **P3HT-*b*-PTP** increasing, the H-aggregate model of Spano et al. was referred. The free exciton bandwidth (W) within the crystalline phase can be calculated from the intensity ratio (A) of the A_{0-0} to A_{0-1} absorbance bands via the relation: [42,55]

$$A = \frac{A_{0-0}}{A_{0-1}} = \left(\frac{1 - 0.24W / E_P}{1 + 0.073W / E_P} \right)^2$$

where E_p is the vibrational energy of the main intramolecular transition corresponding to a symmetric vinyl stretch (assumed to be 180 eV). The calculated free exciton bandwidth W presented in **Table 4** shows that the W decreased with increasing the

P3HT-*b*-PTP fraction ratio in the range of 1-5 wt%. According to Clark et al.,[58] a decrease in *W* (manifested in the spectra as an increase in A), assuming similar interchain ordering, would be consistent with an increase in the effective conjugation length (more linearized, better ordered polymer chains). Thereby, the enhanced P3HT chains ordering is found in the P3HT:PCBM: **P3HT-*b*-PTP** blends with the **P3HT-*b*-PTP** fraction ratio in the range of 1-5 wt%, and the most orderly P3HT chains arrangement achieves when 5 wt% **P3HT-*b*-PTP** is incorporated inducing by the spontaneous assembly of liquid crystalline block copolymer **P3HT-*b*-PTP** upon liquid crystalline state thermal treatment. This result confirms that the self-assembly of liquid crystalline block copolymer **P3HT-*b*-PTP** incorporated into the P3HT:PCBM active layer was involved in improving crystallization and ordering of P3HT chains, thus the favoring charge mobility, J_{sc}, FF and PCE.

For the sake of get insight into the nanomorphology of the active layers and how the orientation of P3HT chains is influenced by various fraction of **P3HT-*b*-PTP** after annealed at 150 ^{o}C, out-of-plane (q_z) grazing incidence X-ray diffraction (GIXRD) measurement has been carried out on the active layers, as depicted in **Figure 5**. The diffraction peaks located at 2θ = 5.5°, 10.8° and 16.4° corresponding to the (100), (200) and (300) reflections of the lamellae, respectively. In the lamellar-stacking structure of P3HT, alkyl side chains of P3HT are oriented vertical to the substrate to form an edge-on orientation, where P3HT chains along the crystallographic direction is perpendicular to the backbone, and the intermolecular π-π stacking between the thiophene rings is parallel to the substrate, which usually providing the (100) diffraction peak in the out-of-plane (q_z) direction.[13,21,43,57] The intensity of P3HT (100) reflection slightly increases with the addition of 5% weight ratio of P3HT-b-PTP, while the value decreases with a higher weight ratio (10%) of P3HT-b-PTP. The increased intensity is demonstrative of an improvement in P3HT crystallinity, which is in accordance with the UV-vis result.

The AFM images of 5 μm × 5 μm region of the active layers with various fractions of **P3HT-*b*-PTP** after annealed at 150 ^{o}C are shown in **Figure 6**. The RMS roughness of the pristine P3HT:PCBM active layer is 2.9 nm. Incorporation of 1, 3 and 5 wt % of

liquid crystalline block copolymer **P3HT-*b*-PTP** decreases the RMS roughness of the active layers to 2.6, 2.1 and 1.8 nm, respectively. The active layers with 3 and 5 wt % of **P3HT-*b*-PTP** show the finer nanoscale morphologies than the one with 1% wt% of **P3HT-*b*-PTP**. This finer nanomorphology can provide good contact between the electrodes and active layer, resulting in more efficient charge transport, as well as the reduced R_s (**Table 4**), which is correlated to improve J_{sc}, FF, and PCE.[59] Further increase the weigth ratio of **P3HT-*b*-PTP** to 10 wt %, a rougher surface morphology was observed together with a RMS roughness of 4.3 nm, which may lead to an unfavorable condition for charge separation and transport, thus decreasing the PCE.[60] The similar results also happened in the case of active layer with **P3HT-*b*-Pterph** (**Figure S15**).

Facilitated exciton dissociation and charge transfer was performed by the steady-state photoluminescence (PL) measurements of the active layers (**Figure 7** and **Figure S16**). The PL emission peak of P3HT located at around 640 nm is ascribed to the radiative decay of excitons to ground state. The PL spectrum intensity is significantly quenched after blended with PCBM. Incorporation of 1-5 wt% of **P3HT-*b*-Pterph** or **P3HT-*b*-PTP** further quenches the PL emission, due to a more efficient exciton dissociation process.[50,61] These charge-transfer dynamics were further supported by time-resolved photoluminescence (TRPL) (**Figure 7**). The fitted lifetime of the active layers for pristine P3HT:PCBM and P3HT:PCBM with 1, 3, 5, 10 wt% of **P3HT-*b*-PTP** are 470, 360, 310, 280, 510 ps, respectively. The shorter exciton lifetime of the active layers with **P3HT-*b*-PTP** indicates the faster exciton dissociation. The improved charge separation efficiency gives rise to J_{sc} and photovoltaic performance.

It is well-known that the orientation and crystallinity of the P3HT chain could influence the carrier mobility of active layers.[62-64] Therefore, the hole and electron transport behaviors of the active layers with and without liquid crystalline block copolymer compatibilizer after annealed at 150 ^{o}C were investigated according to the Mott−Gurney space-charge-limited-current (SCLC) law:[65,66]

$$J=(9/8)\mu\varepsilon_0\varepsilon_r(V^2/L^3)$$

Where J = current density, μ = hole or electron mobility, ε_0 = vacuum permittivity, ε_r = permittivity of active layer, and L = the thickness of the active layer. $V = V_{appl} - V_{bi} - V_r$, where V_{appl} = applied voltage to the device, V_{bi} = built-in voltage induced by the different work function between the two electrodes, V_r = voltage drop caused by the series resistance. **Figure 8** shows the hole only J-V characteristics of the active layers with and without liquid crystalline block copolymer compatibilizer, insets presented the device architecture and $J^{0.5}$ vs V plots for Mott-Gurney SCLC fitting. The hole mobility increases with the addition of 1-5 wt% **P3HT-*b*-PTP**. The corresponding estimated hole mobility for pristine P3HT:PCBM and P3HT:PCBM with 1, 3, 5, 10 wt% of **P3HT-*b*-PTP** are 2.16×10^{-8} and 2.97×10^{-8}, 2.97×10^{-8}, 4.27×10^{-8}, 1.63×10^{-8} $m^2 V^{-1}s^{-1}$ respectively. Similarly, the maximum of electron mobility $\mu_e = 8.34\times10^{-8}$ $m^2 V^{-1}s^{-1}$ is achieved when incorporation 5 wt% of **P3HT-*b*-PTP** (**Figure 8**). These fitting hole and electron mobility values are summarized in **Table 5**. The increased hole and electron mobility is consistent with the improved orientation and crystallinity of the P3HT chain, which is important for the promotion of the photovoltaic performance.

Conductive atomic force microscopy (CAFM) measurements were employed to determine the electronic conductivities of the active layers. **Figure 9** shows the CAFM current images of the pristine P3HT:PCBM and P3HT:PCBM with 5 wt % **P3HT-*b*-PTP** active layers of a 5 μm × 5 μm surface scan area. The mean current of the P3HT:PCBM active layer increases from 12.6 to 26.3 pA after incorporation of 5 wt % liquid crystalline block copolymer compatibilizer. This high electronic conductivity comes from the enhanced orientation and crystallinity of the P3HT chain, which will facilitate charge transport and contribute to the improvement in J_{sc} and PCE.[50,67]

Conclusions

In summary, the application of P3HT based self-assemble liquid crystalline rod-coil block copolymers **P3HT-*b*-Pterph** and **P3HT-*b*-PTP** in solar cells has been investigated. Incorporation of the low conductive non-conjugated liquid crystalline

block into the copolymers resulted in poor photovoltaic performance of the solar cells based on **P3HT-*b*-Pterph** or **P3HT-*b*-PTP** blended with PCBM. On the other hand, when utilize the liquid crystalline rod-coil block copolymers as compatibilizers in P3HT:PCBM blends, the photovoltaic performance of P3HT:PCBM solar cells can be significantly improved at the optimal concentration of liquid crystalline rod-coil block copolymers, especially after annealing from the liquid crystalline states. The self-assembly of liquid crystalline block, the molecule-block interaction between P3HT block and P3HT chains and the liquid crystalline copolymer located at the interface of donor and acceptor can induce a long range crystallinity of P3HT domains and the formation of interpenetrating networks, which resulted in the improved charge transport. Overall, using the liquid crystalline block copolymers as compatibilizers in the BHJ provides a promising approach to improve the photovoltaic performance by optimizing the nanomorphology of the active layer.

ACKNOWLEDGEMENTS

This work was supported by the National Natural Science Foundation of China (51273088 and 51263016).

References

(1) Li, G.; Zhu, R.; Yang, Y. *Nat Photon* **2012**, *6*, 153.

(2) Günes, S.; Neugebauer, H.; Sariciftci, N. S. *Chem Rev* **2007**, *107*, 1324.

(3) Heeger, A. J. *Chem Soc Rev* **2010**, *39*, 2354.

(4) Krebs, F. C.; Espinosa, N.; Hösel, M.; Søndergaard, R. R.; Jørgensen, M. *Adv Mater* **2014**, *26*, 29.

(5) He, Z.; Zhong, C.; Su, S.; Xu, M.; Wu, H.; Cao, Y. *Nat Photon* **2012**, *6*, 593.

(6) Liu, S.; Zhang, K.; Lu, J.; Zhang, J.; Yip, H.-L.; Huang, F.; Cao, Y. *J Am Chem Soc* **2013**, *135*, 15326.

(7) You, J.; Dou, L.; Yoshimura, K.; Kato, T.; Ohya, K.; Moriarty, T.; Emery, K.; Chen, C. C.; Gao, J.; Li, G.; Yang, Y. *Nat Commun* **2013**, *4*, 1446.

(8) Dang, M. T.; Hirsch, L.; Wantz, G.; Wuest, J. D. *Chem Rev* **2013**, *113*, 3734.

(9) Sun, Z.; Xiao, K.; Keum, J. K.; Yu, X.; Hong, K.; Browning, J.; Ivanov, I. N.; Chen, J.; Alonzo, J.; Li, D.; Sumpter, B. G.; Payzant, E. A.; Rouleau, C. M.; Geohegan, D. B. *Adv Mater* **2011**, *23*, 5529.

(10) Chen, W.; Nikiforov, M. P.; Darling, S. B. *Energ Environ Sci* **2012**, *5*, 8045.

(11) Son, H. J.; Carsten, B.; Jung, I. H.; Yu, L. P. *Energ Environ Sci* **2012**, *5*, 8158.

(12) He, F.; Yu, L. *J Phys Chem Lett* **2011**, *2*, 3102.

(13) Deribew, D.; Pavlopoulou, E.; Fleury, G.; Nicolet, C.; Renaud, C.; Mougnier, S.-J.; Vignau, L.; Cloutet, E.; Brochon, C.; Cousin, F.; Portale, G.; Geoghegan, M.; Hadziioannou, G. *Macromolecules* **2013**, *46*, 3015.

(14) Darling, S. B. *Energ Environ Sci* **2009**, *2*, 1266.

(15) Venkataraman, D.; Yurt, S.; Venkatraman, B. H.; Gavvalapalli, N. *J Phys Chem Lett* **2010**, *1*, 947.

(16) Yassar, A.; Miozzo, L.; Gironda, R.; Horowitz, G. *Prog Polym Sci* **2013**, *38*, 791.

(17) Robb, M. J.; Ku, S.-Y.; Hawker, C. J. *Adv Mater* **2013**, *25*, 5686.

(18) Stalmach, U.; de Boer, B.; Videlot, C.; van Hutten, P. F.; Hadziioannou, G. *J Am Chem Soc* **2000**, *122*, 5464.

(19) Sary, N.; Richard, F.; Brochon, C.; Leclerc, N.; Lévêque, P.; Audinot, J.-N.; Berson, S.; Heiser, T.; Hadziioannou, G.; Mezzenga, R. *Adv Mater* **2010**, *22*, 763.

(20) Botiz, I.; Darling, S. B. *Macromolecules* **2009**, *42*, 8211.

(21) Renaud, C.; Mougnier, S. J.; Pavlopoulou, E.; Brochon, C.; Fleury, G.; Deribew, D.; Portale, G.; Cloutet, E.; Chambon, S.; Vignau, L.; Hadziioannou, G. *Adv Mater* **2012**, *24*, 2196.

(22) Han, M.; Kim, H.; Seo, H.; Ma, B.; Park, J. W. *Adv Mater* **2012**, *24*, 6311.

(23) Sivula, K.; Ball, Z. T.; Watanabe, N.; Fréchet, J. M. J. *Adv Mater* **2006**, *18*, 206.

(24) Yang, D. K.; Wu., S. T. *Fundamentals of Liquid Crystal Devices*; NewYork, Wiley, 2006.

(25) Han, D.; Tong, X.; Zhao, Y.; Zhao, Y. *Angew Chem Int Ed Engl* **2010**, *49*,

9162.

(26) Tong, X.; Han, D.; Fortin, D.; Zhao, Y. *Adv Funct Mater* **2013**, *23*, 204.

(27) Schmidt-Mende, L.; Fechtenkötter, A.; Müllen, K.; Moons, E.; Friend, R. H.; MacKenzie, J. D. *Science* **2001**, *293*, 1119.

(28) Kang, S. J.; Ahn, S.; Kim, J. B.; Schenck, C.; Hiszpanski, A. M.; Oh, S.; Schiros, T.; Loo, Y.-L.; Nuckolls, C. *J Am Chem Soc* **2013**, *135*, 2207.

(29) Parmer, J. E.; Mayer, A. C.; Hardin, B. E.; Scully, S. R.; McGehee, M. D.; Heeney, M.; McCulloch, I. *Appl Phys Lett* **2008**, *92*, 113309.

(30) Zhou, D.; Chen, Y.; Chen, L.; Zhou, W.; He, X. *Macromolecules* **2009**, *42*, 1454.

(31) Chen, L.; Chen, Y.; Yao, K.; Zhou, W.; Li, F.; Chen, L.; Hu, R.; Tang, B. Z. *Macromolecules* **2009**, *42*, 5053.

(32) Chen, L.; Chen, Y.; Zhou, D.; Li, F.; Zha, D.; Yao, K. *Macromol Chem Physic* **2011**, *212*, 24.

(33) Yuan, K.; Li, F.; Chen, L.; Li, Y.; Chen, Y. *J Phys Chem C* **2012**, *116*, 6332.

(34) Yao, K.; Chen, Y.; Chen, L.; Zha, D.; Li, F.; Pei, J.; Liu, Z.; Tian, W. *J Phys Chem C* **2010**, *114*, 18001.

(35) Yao, K.; Chen, Y.; Chen, L.; Li, F.; Li, X.; Ren, X.; Wang, H.; Liu, T. *Macromolecules* **2011**, *44*, 2698.

(36) Chen, X.; Chen, L.; Yao, K.; Chen, Y. *ACS Appl Mater Interfaces* **2013**, *5*, 8321.

(37) Iovu, M. C.; Jeffries-El, M.; Sheina, E. E.; Cooper, J. R.; McCullough, R. D. *Polymer* **2005**, *46*, 8582.

(38) Liu, J.; Haynes, D.; Balliet, C.; Zhang, R.; Kowalewski, T.; McCullough, R. D. *Adv Funct Mater* **2012**, *22*, 1024.

(39) Wu, B.; Mu, B.; Wang, S.; Duan, J.; Fang, J.; Cheng, R.; Chen, D. *Macromolecules* **2013**, *46*, 2916.

(40) Xing, C.; Lam, J. W. Y.; Zhao, K.; Tang, B. Z. *J Polym Sci Pol Chem* **2008**, *46*, 2960.

(41) Tahar-Djebbar, I.; Nekelson, F.; Heinrich, B.; Donnio, B.; Guillon, D.; Kreher,

D.; Mathevet, F.; Attias, A.-J. *Chem Mater* **2011**, *23*, 4653.

(42) Crossland, E. J. W.; Rahimi, K.; Reiter, G.; Steiner, U.; Ludwigs, S. *Adv Funct Mater* **2011**, *21*, 518.

(43) Aiyar, A. R.; Hong, J. I.; Nambiar, R.; Collard, D. M.; Reichmanis, E. *Adv Funct Mater* **2011**, *21*, 2652.

(44) Lee, E.; Hammer, B.; Kim, J. K.; Page, Z.; Emrick, T.; Hayward, R. C. *J Am Chem Soc* **2011**, *133*, 10390.

(45) Grancharov, G.; Coulembier, O.; Surin, M.; Lazzaroni, R.; Dubois, P. *Macromolecules* **2010**, *43*, 8957.

(46) Watanabe, M.; Tsuchiya, K.; Shinnai, T.; Kijima, M. *Macromolecules* **2012**, *45*, 1825.

(47) Yip, H.-L.; Jen, A. K. Y. *Energ Environ Sci* **2012**, *5*, 5994.

(48) Kumar, A.; Sista, S.; Yang, Y. *J Appl Phys* **2009**, *105*.

(49) Hartmann, L.; Tremel, K.; Uttiya, S.; Crossland, E.; Ludwigs, S.; Kayunkid, N.; Vergnat, C.; Brinkmann, M. *Adv Funct Mater* **2011**, *21*, 4047.

(50) Lu, L.; Xu, T.; Chen, W.; Lee, J. M.; Luo, Z.; Jung, I. H.; Park, H. I.; Kim, S. O.; Yu, L. *Nano Lett* **2013**, *13*, 2365.

(51) You, J.; Chen, C. C.; Dou, L.; Murase, S.; Duan, H. S.; Hawks, S. A.; Xu, T.; Son, H. J.; Yu, L.; Li, G.; Yang, Y. *Adv Mater* **2012**, *24*, 5267.

(52) Oh, J. Y.; Shin, M.; Lee, T. I.; Jang, W. S.; Min, Y.; Myoung, J.-M.; Baik, H. K.; Jeong, U. *Macromolecules* **2012**, *45*, 7504.

(53) Brinkmann, M.; Chandezon, F.; Pansu, R. B.; Julien-Rabant, C. *Adv Funct Mater* **2009**, *19*, 2759.

(54) Nagarjuna, G.; Baghgar, M.; Labastide, J. A.; Algaier, D. D.; Barnes, M. D.; Venkataraman, D. *ACS Nano.* **2012**, *6*, 10750.

(55) Clark, J.; Silva, C.; Friend, R. H.; Spano, F. C. *Phys Rev Lett* **2007**, *98*, 206406.

(56) Brown, P. J.; Thomas, D. S.; Köhler, A.; Wilson, J. S.; Kim, J.-S.; Ramsdale, C. M.; Sirringhaus, H.; Friend, R. H. *Phys Rev B* **2003**, *67*, 064203.

(57) Lin, Y.; Lim, J. A.; Wei, Q.; Mannsfeld, S. C. B.; Briseno, A. L.; Watkins, J. J.

Chem Mater **2012**, *24*, 622.

(58) Clark, J.; Chang, J.-F.; Spano, F. C.; Friend, R. H.; Silva, C. *Appl Phys Lett* **2009**, *94*, 163306.

(59) Griffini, G.; Douglas, J. D.; Piliego, C.; Holcombe, T. W.; Turri, S.; Frechet, J. M.; Mynar, J. L. *Adv Mater* **2011**, *23*, 1660.

(60) Lobez, J. M.; Andrew, T. L.; Bulovic, V.; Swager, T. M. *ACS Nano.* **2012**, *6*, 3044.

(61) Bansal, N.; Reynolds, L. X.; MacLachlan, A.; Lutz, T.; Ashraf, R. S.; Zhang, W.; Nielsen, C. B.; McCulloch, I.; Rebois, D. G.; Kirchartz, T.; Hill, M. S.; Molloy, K. C.; Nelson, J.; Haque, S. A. *Sci Rep* **2013**, *3*, 1531.

(62) Lin, C.-C.; Ho, P.-H.; Huang, C.-L.; Du, C.-H.; Yu, C.-C.; Chen, H.-L.; Yeh, Y.-C.; Li, S.-S.; Lee, C.-K.; Pao, C.-W.; Chang, C.-P.; Chu, M.-W.; Chen, C.-W. *J Phys Chem C* **2012**, *116*, 25081.

(63) Kline, R. J.; McGehee, M. D. *J. Macromol. Sci., Polymer. Rev* **2006**, *46*, 27.

(64) Kim, D. H.; Park, Y. D.; Jang, Y.; Yang, H.; Kim, Y. H.; Han, J. I.; Moon, D. G.; Park, S.; Chang, T.; Chang, C.; Joo, M.; Ryu, C. Y.; Cho, K. *Adv Funct Mater* **2005**, *15*, 77.

(65) Goh, C.; Kline, R. J.; McGehee, M. D.; Kadnikova, E. N.; Frechet, J. M. J. *Appl Phys Lett* **2005**, *86*, 122110.

(66) Zhang, X. G.; Pantelides, S. T. *Phys Rev Lett* **2012**, *108*, 266602.

(67) Yang, T.; Wang, M.; Duan, C.; Hu, X.; Huang, L.; Peng, J.; Huang, F.; Gong, X. *Energ Environ Sci* **2012**, *5*, 8208.

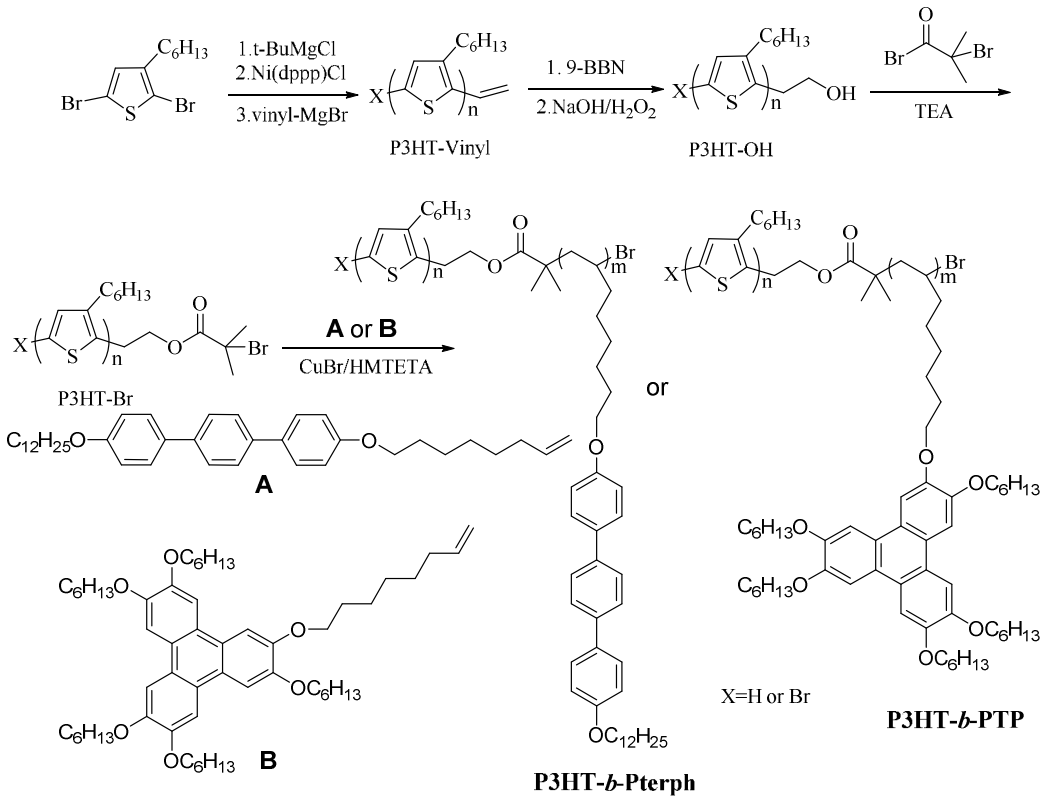

Scheme 1. Synthesis of **P3HT-*b*-Pterph** and **P3HT-*b*-PTP**.

Table 1. Physical, optical properties and energy levels summary of liquid crystalline block copolymers.

Compounds	T_d[a] (°C)	mesophase[b] (°C)	UV-vis/PL max film (nm) [c]	E_{OX} vs Ag/Ag^+ (V)[d]	E_{HOMO} (eV)[e]	E_{LUMO} (eV)[f]
P3HT-*b*-Pterph	416	172-178	561/642	0.64	-5.35	-3.47
P3HT-*b*-PTP	403	147-154	559/637	0.59	-5.30	-3.40

[a] From TGA, heating rate of 10 °C/min under nitrogen until weight loss of 5%. [b] From DSC, heating rate of 5 °C/min under nitrogen. [c] Spin-coated from 1,2-dichlorobenzene solution. [d] Drop-cast from 1,2-dichlorobenzene solution on a platinum working electrode. [e] E_{HOMO} was calculated from onset oxidation potential E_{ox} according to the equation: $E_{HUMO} = -(E_{ox} + 4.71)$ (eV). [f] E_{LUMO} calculated from the E_{HOMO} and the UV-vis absorption onset (optical bandgap).

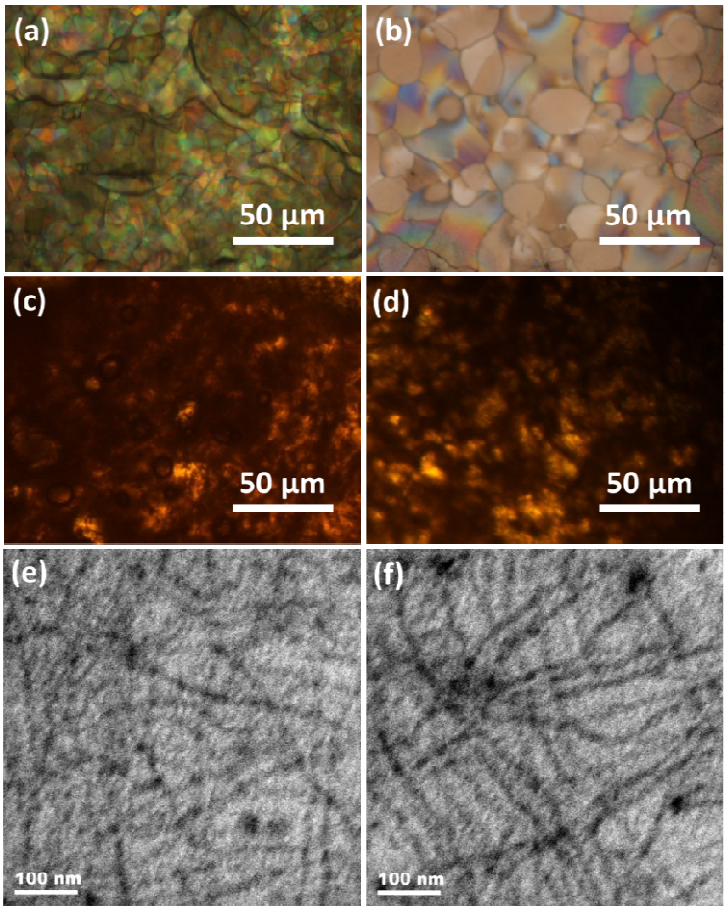

Figure 1. Polarized optical micrographs of (a) terph-vinyl (b) TP-vinyl (c) **P3HT-*b*-Pterph** and (d) **P3HT-*b*-PTP**. TEM images of the self-assemble liquid crystalline block copolymers (e) **P3HT-*b*-Pterph** and (f) **P3HT-*b*-PTP**.

Table 2. Device parameters of **P3HT-*b*-Pterph**/PCBM and **P3HT-*b*-PTP**/PCBM based devices annealed at different temperatures under AM 1.5G illumination.

Device	J_{sc}(mA/cm^2)	V_{oc}(V)	*FF*(%)	PCE(%)	R_s(Ω cm^2)	R_{sh}(Ω cm^2)
P3HT-*b*-Pterph/PCBM	2.83±0.1	0.54±0.01	22.1±1	0.34±0.01	17.6	179.1
Annealed at 120 °C	3.39±0.15	0.54±0.01	21.4±1	0.39±0.01	12.8	213.5
Annealed at 175 °C	4.42±0.15	0.54±0.01	23.6±1	0.56±0.02	11.3	267.3
Annealed at 200 °C	2.41±0.1	0.54±0.01	23.3±1	0.30±0.01	18.5	147.1
P3HT-*b*-PTP/PCBM	3.62±0.1	0.56±0.01	21.8±1	0.44±0.01	17.3	183.8
Annealed at 120 °C	4.53±0.15	0.56±0.01	23.3±1	0.59±0.02	11.7	287.6
Annealed at 150 °C	4.73±0.15	0.56±0.01	23.9±1	0.63±0.02	10.9	319.7
Annealed at 200 °C	3.59±0.1	0.55±0.01	21.1±1	0.42±0.01	19.6	180.3

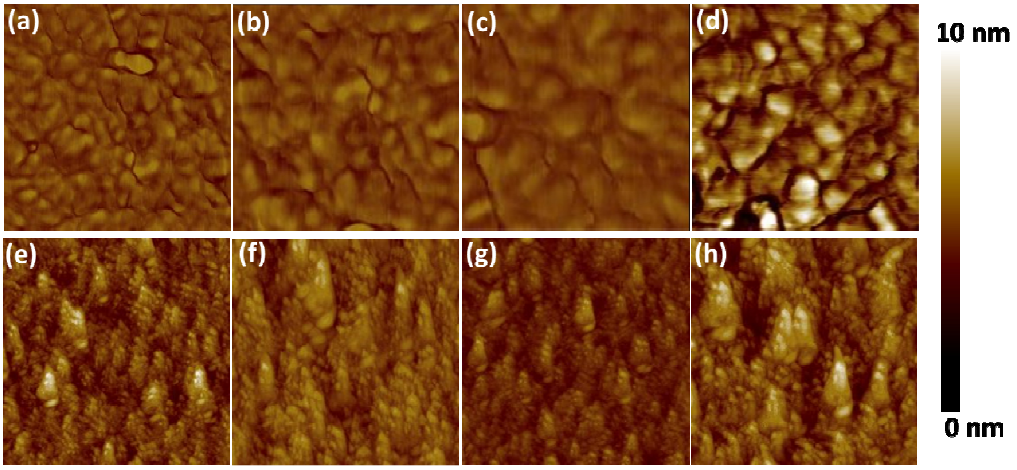

Figure 2. 5 μm × 5 μm tapping-mode AFM topography height images of **P3HT-*b*-Pterph**/PCBM (a) as casted (b) annealed at 120 ^{o}C (c) annealed at 175 ^{o}C (d) annealed at 200 ^{o}C, and **P3HT-*b*-PTP** /PCBM (e) as casted, (f) annealed at 120 ^{o}C, (g) annealed at 150 ^{o}C, (h) annealed at 200 ^{o}C. The thermal treatments are all under N_2 atmosphere.

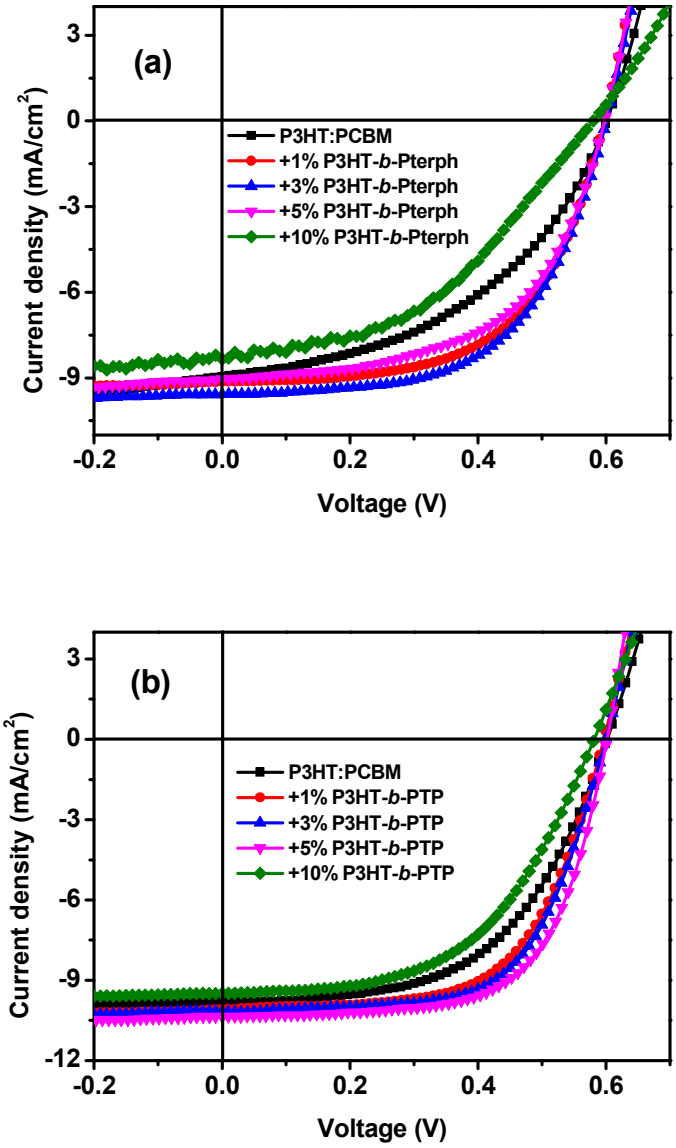

Figure 3. Current density-voltage (*J-V*) curves of (a) P3HT:PCBM and P3HT:PCBM: **P3HT-*b*-Pterph** organic solar cells with various concentrations of **P3HT-*b*-Pterph** after annealed at 175 ^{o}C under N_2 atmosphere. (b) P3HT:PCBM and P3HT:PCBM: **P3HT-*b*-PTP** organic solar cells with various concentrations of **P3HT-*b*-PTP** after annealed at 150 ^{o}C under N_2 atmosphere.

Table 3. Device parameters of P3HT:PCBM:**P3HT-*b*-Pterph** and P3HT:PCBM:**P3HT-*b*-PTP** solar cells with various concentrations of **P3HT-*b*-Pterph** and **P3HT-*b*-PTP** after annealed at 175 °C and 150 °C under N_2 atmosphere, respectively.

Device	J_{sc}(mA/cm^2)	V_{oc}(V)	*FF*(%)	PCE(%)	R_s(Ω cm^2)	R_{sh}(Ω cm^2)
P3HT:PCBM[a]	8.97±0.2	0.60±0.01	45.1±1	2.44±0.1	10.5	351.1
+1% **P3HT-*b*-Pterph**	9.13±0.2	0.60±0.01	58.3±1	3.20±0.1	7.1	771.3
+3% **P3HT-*b*-Pterph**	9.58±0.3	0.60±0.01	58.1±1	3.34±0.15	6.3	942.5
+5% **P3HT-*b*-Pterph**	9.05±0.3	0.60±0.01	55.6±1	3.01±0.15	7.8	769.7
+10% **P3HT-*b*-Pterph**	8.34±0.2	0.58±0.01	43.1±1	2.08±0.1	11.6	446.3
P3HT:PCBM[b]	9.81±0.2	0.60±0.01	55.1±1	3.24±0.1	8.3	728.5
+1% **P3HT-*b*-PTP**	10.11±0.2	0.60±0.01	61.1±1	3.69±0.1	7.6	847.3
+3% **P3HT-*b*-PTP**	10.17±0.3	0.60±0.01	63.2±1	3.86±0.15	6.2	942.6
+5% **P3HT-*b*-PTP**	10.36±0.3	0.60±0.01	64.9±1	4.03±0.15	4.8	1074.2
+10% **P3HT-*b*-PTP**	9.49±0.2	0.58±0.01	53.1±1	2.92±0.1	9.7	656.7

[a] Device after postannealing treatment at 175 °C. [b] Device after postannealing treatment at 150 °C.

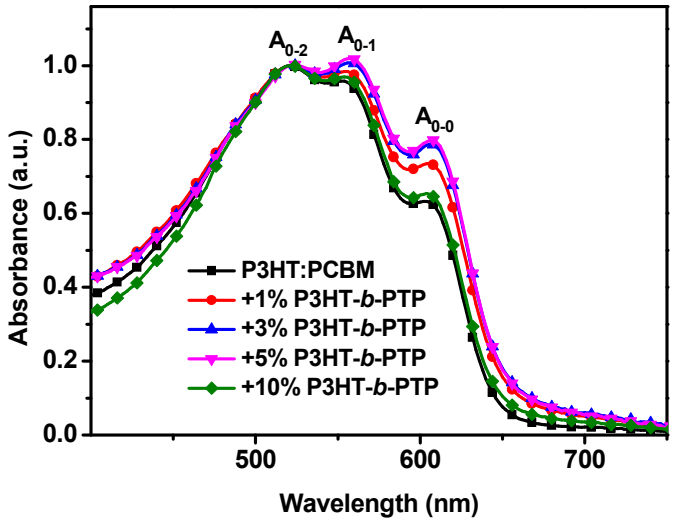

Figure 4. Normalized absorption spectra of P3HT:PCBM and P3HT:PCBM: **P3HT-*b*-PTP** films with various weight ratio of **P3HT-*b*-PTP** after annealed at 150 ^{o}C under N_2 atmosphere.

Table 4. Peak positions of $A_{0\text{-}0}$ and $A_{0\text{-}1}$ transitions from UV-vis absorption spectra, and $A_{0\text{-}0}/A_{0\text{-}1}$ intensity of the active layers with different fractions of **P3HT-*b*-PTP** after annealed at 150 ^{o}C under N_2 atmosphere.

Active layer	$\lambda_{A0\text{-}1}$ (nm)	$\lambda_{A0\text{-}0}$ (nm)	$A_{0\text{-}0}/A_{0\text{-}1}$	W (meV)	$A_{0\text{-}0}/A_{0\text{-}2}$
P3HT:PCBM[b]	555	605	0.66	112.6	0.63
+1% **P3HT-*b*-PTP**	557	607	0.75	78.5	0.74
+3% **P3HT-*b*-PTP**	558	608	0.78	69.1	0.79
+5% **P3HT-*b*-PTP**	558	608	0.78	69.1	0.80
+10% **P3HT-*b*-PTP**	555	605	0.67	109.0	0.65

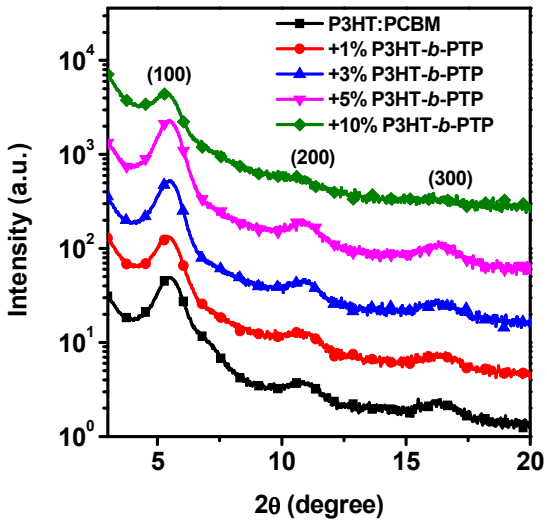

Figure 5. Out-of-plane GIXD profiles of P3HT:PCBM and P3HT:PCBM: **P3HT-*b*-PTP** films with various weight ratio of **P3HT-*b*-PTP** after annealed at 150 ^{o}C under N_2 atmosphere.

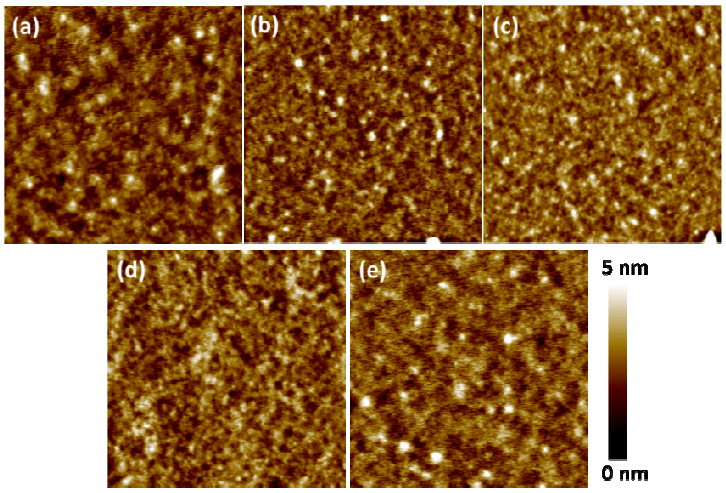

Figure 6. 5 μm × 5 μm tapping-mode AFM topography height images of (a) P3HT:PCBM and P3HT:PCBM:**P3HT-*b*-PTP** films with (b) 1%, (c) 3%, (d) 5%, (e) 10% **P3HT-*b*-PTP** after annealed at 150 ^{o}C under N_2 atmosphere.

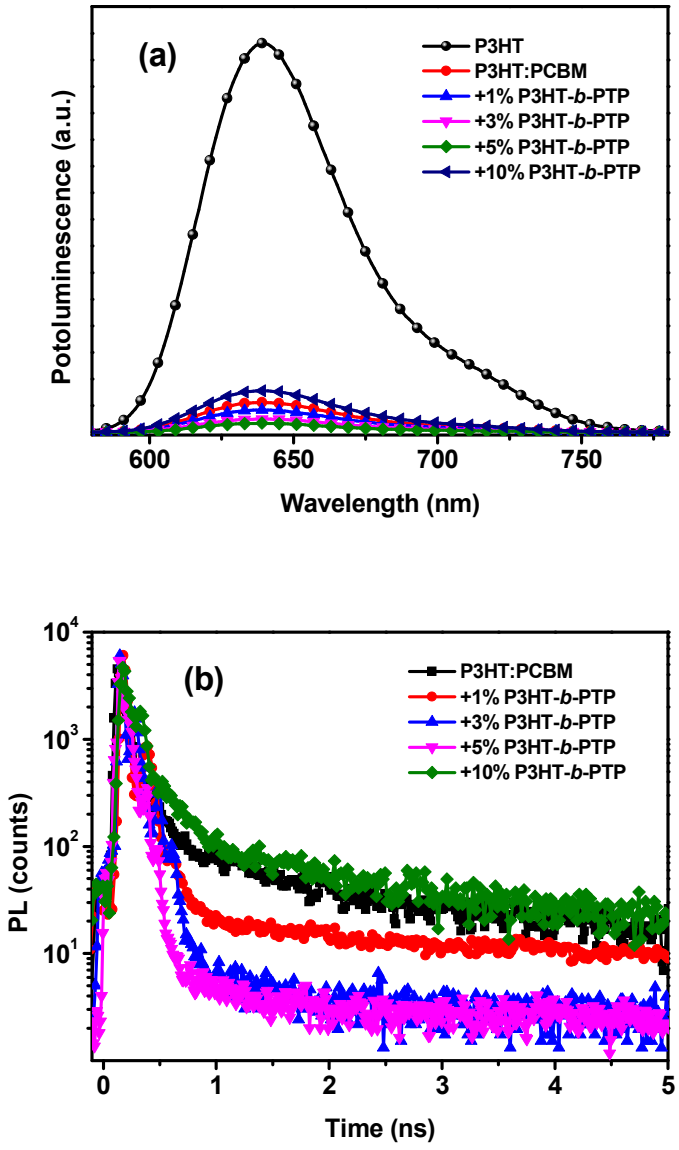

Figure 7. (a) PL spectra of P3HT, P3HT:PCBM and P3HT:PCBM:**P3HT-*b*-PTP** films with various weight ratio of **P3HT-*b*-PTP** after annealed at 150 ^{o}C under N_2 atmosphere. (b) Time-resolved photoluminescence decay spectra of P3HT:PCBM and P3HT:PCBM: **P3HT-*b*-PTP** films with various weight ratio of **P3HT-*b*-PTP** after annealed at 150 ^{o}C under N_2 atmosphere. The fitted lifetime is τ = 470, 360, 310, 280, 510 ps for P3HT:PCBM:**P3HT-*b*-PTP** with 0%, 1%, 3%, 5%, 10% **P3HT-*b*-PTP**, respectively.

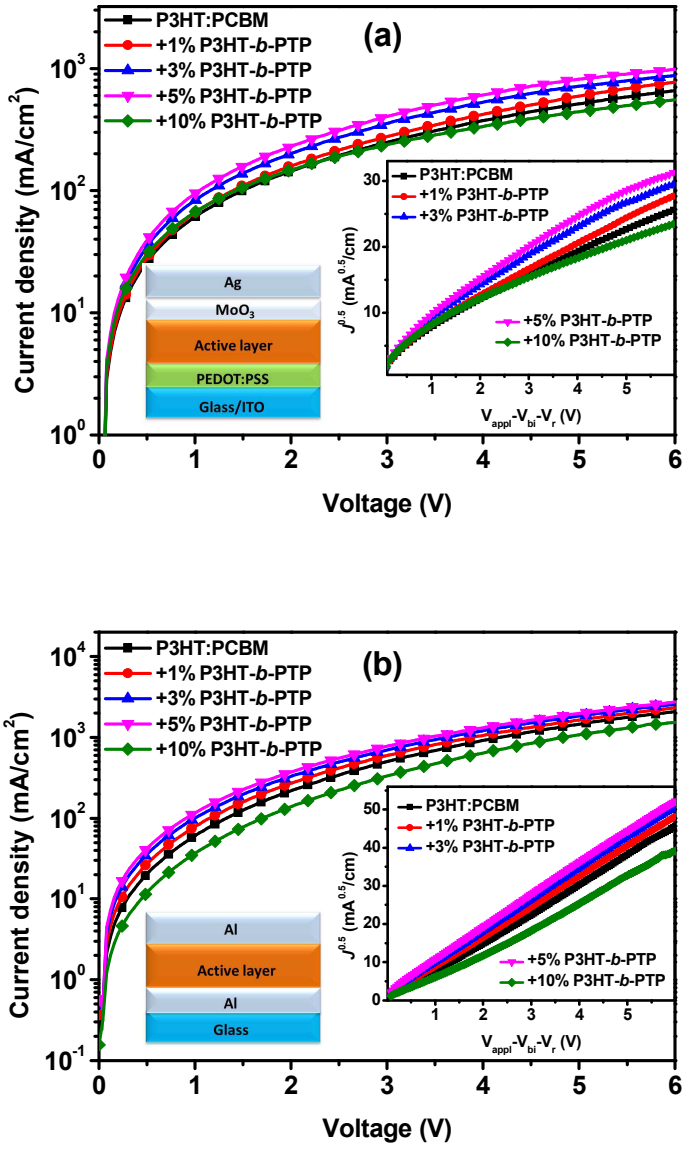

Figure 8. *J* vs *V* plots for (a) hole-only and (b) electron-only devices based on P3HT:PCBM with different weight fractions of **P3HT-*b*-PTP** after annealed at 150 ^{o}C under N_2 atmosphere. Insets: left, (a) hole-only and (b) electron-only device architecture, right, $J^{0.5}$ vs *V* plots for Mott–Gurney SCLC fitting of the (a) hole-only and (b) electron-only devices.

Table 5. Hole mobility (μ_h) and electron mobility (μ_e) calculated by the Mott-Gurney SCLC of devices based on P3HT:PCBM:**P3HT-*b*-PTP** with various weight ratio of **P3HT-*b*-PTP** after annealed at 150 ^oC under N_2 atmosphere.

Active layer	P3HT:PCBM	+1% **P3HT-*b*-PTP**	+3% **P3HT-*b*-PTP**	+5% **P3HT-*b*-PTP**	+10% **P3HT-*b*-PTP**
μ_h ($m^2 V^{-1}s^{-1}$)	2.16×10^{-8}	2.97×10^{-8}	3.83×10^{-8}	4.27×10^{-8}	1.63×10^{-8}
μ_e ($m^2 V^{-1}s^{-1}$)	3.93×10^{-8}	5.27×10^{-8}	7.18×10^{-8}	8.34×10^{-8}	2.29×10^{-8}

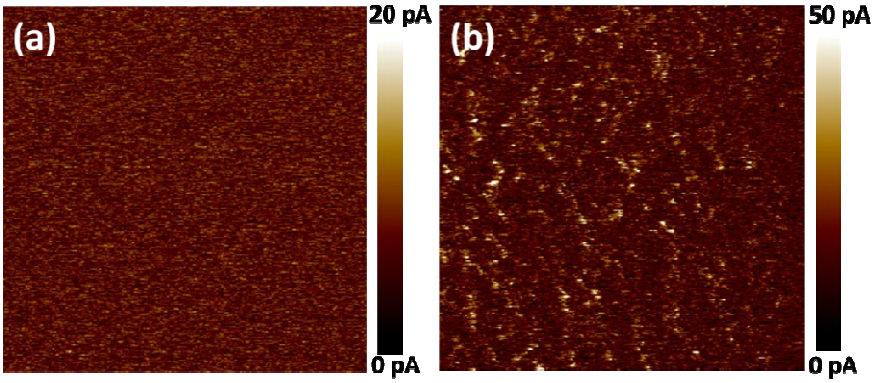

Figure 9. Conductive atomic force microscopy (CAFM) of (a) pristine P3HT:PCBM and (b) P3HT:PCBM: **P3HT-*b*-PTP** with 5% **P3HT-*b*-PTP** films. The scan area was 5 μm × 5 μm.

Table of contents

Photovoltaic Performance Enhancement of P3HT/PCBM Solar Cells Driven by Incorporation of Conjugated Liquid Crystalline Rod-coil Block Copolymers

Kai Yuan, Lie Chen, Yiwang Chen

Liquid crystalline rod-coil block copolymer compatibilizers are applied in polymer solar cells for modifying the interface between P3HT and PCBM.